# Phase transitions in thin mesoscopic superconducting disks

V. A. Schweigert* and F. M. Peeters†
*Departement Natuurkunde, Universiteit Antwerpen (UIA), Universiteitsplein 1, B-2610 Antwerpen, Belgium*
(Received 4 December 1997)

Phase transitions between different superconducting states and between the superconducting-normal state of mesoscopic disks are studied by solving the two Ginzburg-Landau (GL) equations self-consistently. We limit ourselves to superconducting states with a fixed angular momentum for disks thinner than the coherence length. We find that the type of phase transition depends on the disk size, namely, *both* the radius and the thickness. Using an expansion over the eigenfunction of the linearized first GL equation, we develop an analytical approach that allows us to predict the type of phase transition and find the system characteristics near the phase transition point. The analytical results are in good agreement with results from our simulation obtained by using finite-difference techniques to solve the nonlinear GL equations coupled to the three-dimensional Maxwell equations. A new type of first-order phase transition between different superconducting states having the same angular momentum is predicted. [S0163-1829(98)05221-7]

## I. INTRODUCTION

Modern microfabrication techniques enable one to create very small superconducting structures with unique properties. The behavior of such structures in an external magnetic field is strongly influenced by the boundary conditions and may lead to new superconducting states. In a circular system the superconducting state is characterized by a definite angular momentum that is similar to the Little-Parks oscillations[1] observed in a thin-film cylinder in the presence of an axial field. The angular momentum is just the number of flux quanta trapped by the disk. Transitions between the superconducting states with different angular momentum occur when the magnetic field and/or the temperature is changed. Such transitions are of first order and are accompanied by jumps in the magnetic moment and latent heat. These transitions between different superconducting states in multiply connected systems were studied by Bezryadin and co-workers.[2]

In this paper, we study the properties of superconducting thin-film disks in the presence of a perpendicular magnetic field. Previous investigations[3,4] were limited to the vicinity of the phase transition where the Ginzburg-Landau (GL) equations can be linearized, simplifying the problem considerably. Here we include the nonlinear term and investigate the properties of superconducting disks near the phase boundary. Although the GL equations were derived to describe superconductivity near the critical point, later work has found that this theory is valid over a much broader range of magnetic field and temperature. For the system under study we found that the finite thickness of the disk influences the magnetic-field profile, i.e., the magnetic pressure, and this changes the size of the Meissner effect that is different from the well-studied cylinder geometries.[5]

The type of a superconductor is determined by the value of the GL parameter $\kappa$.[6] For bulk samples we are dealing with a type-I superconductor when $\kappa<1/\sqrt{2}$. When $\kappa<0.42$, the superconducting state with a complete Meissner effect takes place for magnetic fields smaller than the critical value $H_c$ while the normal state is energetically favorable at $H>H_c$. For $0.42<\kappa<1/\sqrt{2}=0.707$, surface superconductivity exists when $H_c<H<H_{c3}$, but the bulk of the sample still remains in the normal state. For type-II superconductors ($\kappa>1/\sqrt{2}$), the Abrikosov vortex lattice is energetically favorable in the range $H_c<H<H_{c2}$. Since the type of superconductor is determined by the competition between the magnetic energy and the condensation energy, one would expect that the behavior of mesoscopic superconducting samples that disturb weakly the applied magnetic field will depend crucially on the size of the sample. Indeed, the experimental observations of the magnetization of mesoscopic disks performed by Geim *et al.*[7] have shown that the *type* and the *order* of the phase transition between the superconducting state and the normal state changes with variation of the disk radius and thickness while keeping the superconducting material the same. A second-order reversible phase transition was observed for small disk radii. With increasing the disk radius the transition between the superconducting state and the normal state is followed by a jump in the magnetization indicating a first-order transition.

In the present work, we mainly consider the case $\kappa<0.42$, when a macroscopic sample exhibits properties inherent for a type-I superconductor. Nevertheless, we find that the type of phase transition between the superconducting and the normal state is determined by the disk thickness. Furthermore, the superconducting state itself can exhibit first-order transitions that are related to different angular momentum giant vortex states.

The paper is organized as follows. In Sec. II, we present the theoretical model and our finite-difference approach to solve the GL equations. The results of a linear analysis of the first GL equation for the order parameter are discussed in Sec. III. In Sec. IV, we develop an analytical approach, which allows us to treat switching between the different types of phase transitions, and we compare these results with those of our numerical calculations. The system characteristics at the first-order transitions, which are found using both the analytical approach and the finite-difference technique, are presented in Sec. V. Section VI is devoted to the behavior of large disks, in which transitions between different su-

 

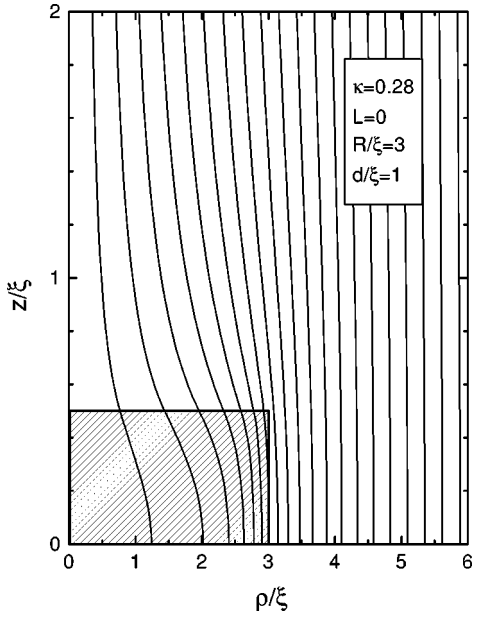


FIG. 1. The magnetic-field distribution for an applied magnetic field of $H_0=0.5H_{c2}$. We took the GL parameter $\kappa=0.28$, the disk radius $R/\xi=3$, the disk thickness $d/\xi=1$, and zero angular momentum. The shaded area corresponds to a quarter of the disk.

perconducting states can take place. Our results are summarized in Sec. VII.

## II. MODEL AND NUMERICAL APPROACH

We consider a superconducting disk with radius $R$ and thickness $d$ immersed in an insulator media (see Fig. 1), which, for example, can also be a vacuum, and which is placed in a perpendicular magnetic field. In the present paper we will solve the system of two coupled GL equations

$$\frac{1}{2m}\left(-i\hbar\vec{\nabla}-\frac{2e\vec{A}}{c}\right)^2\Psi=-\alpha\Psi-\beta\Psi|\Psi|^2, \tag{1}$$

$$\vec{\nabla}\times\vec{\nabla}\times\vec{A}=\frac{4\pi}{c}\vec{j}, \tag{2}$$

where the density of the superconducting current $\vec{j}$ is given by

$$\vec{j}=\frac{e\hbar}{im}(\Psi^*\vec{\nabla}\Psi-\Psi\vec{\nabla}\Psi^*)-\frac{4e^2}{mc}|\Psi|^2\vec{A}. \tag{3}$$

The boundary condition corresponding to zero current density in the insulator media is

$$\left(-i\hbar\vec{\nabla}-\frac{2e\vec{A}}{c}\right)\Big|_n\Psi=0, \tag{4}$$

where the subscript $n$ denotes the component normal to the disk surface. The boundary condition for the vector potential has to be taken far away from the disk

$$\vec{A}_{|\vec{r}\to\infty}=\tfrac{1}{2}\vec{e}_\phi H_0\rho, \tag{5}$$

where the applied magnetic field is uniform and directed normal to the disk plane $\vec{H}=(0,0,H_0)$. Here $\vec{e}_\phi$ denotes the azimuthal direction, $\rho$ is the radial distance from the disk center, and $\vec{r}=(\vec{\rho},z)$ is the three-dimensional position in space.

Using dimensionless variables and the London gauge, $\mathrm{div}\vec{A}=0$, we rewrite the system of equations (1)–(4) in the following form:

$$(-i\vec{\nabla}-\vec{A})^2\Psi=\Psi(1-|\Psi|^2), \tag{6}$$

$$-\kappa^2\triangle\vec{A}=\frac{1}{2i}(\Psi^*\vec{\nabla}\Psi-\Psi\vec{\nabla}\Psi^*)-|\Psi|^2\vec{A}. \tag{7}$$

Here the distance is measured in units of the coherence length $\xi=\hbar/\sqrt{-2m\alpha}$, the order parameter in $\psi_0=\sqrt{-\alpha/\beta}$, the vector potential in $c\hbar/2e\xi$, $\kappa=\lambda/\xi$ is the Ginzburg-Landau parameter, and $\lambda=c\sqrt{m/\pi}/4e\psi_0$ is the penetration length. We measure the magnetic field in $H_{c2}=c\hbar/2e\xi^2=\kappa\sqrt{2}H_c$, where $H_c=\sqrt{-4\pi\alpha/\beta}$ is the critical field. The difference between the superconducting and the normal-state Gibbs free energy measured in $H_c^2V/8\pi$ can be expressed through the integral

$$F=\frac{1}{V}\int[2(\vec{A}-\vec{A}_0)\vec{j}-|\Psi|^4]d\vec{r}, \tag{8}$$

over the disk volume $V=\pi R^2d$, where $\vec{A}_0=\vec{e}_\phi H_0\rho/2$ is the external vector potential in the absence of a superconductor (i.e., with uniform magnetic field), $\vec{j}=[(\Psi^*\vec{\nabla}\Psi-\Psi\vec{\nabla}\Psi^*)/2i-|\Psi|^2\vec{A}]$ is the dimensionless superconducting current. For nonzero temperature $T$, the coherence length is proportional to $(1-T/T_0)^{-1/2}$ and $H_{c2}\sim(1-T/T_0)$, where $T_0$ is the critical temperature corresponding to the transition to the normal state at zero magnetic field. This scaling allows us to relate the numerical results to the experimental measurements performed at nonzero temperature.

We restrict ourselves to thin disks such that $d<\xi$. For the rest there are no other limitations on the disk size. For very thin disks, the magnetic field is uniformly distributed along the $z$ direction. When the disk thickness becomes comparable to the penetration length, the magnetic field is expelled from the disk due to the Meissner effect (see Fig. 1). The field penetrates only a distance $\lambda$ inside the disk. As a consequence, the longitudinal variation of the vector potential becomes rather strong for $d>\lambda$. Nevertheless, we found that this does not lead to important longitudinal variations of the order parameter in disks that are thinner than the coherence length.[8] Representing the order parameter as a series over cosines

$$\Psi(z,\vec{\rho})=\sum_k\ \cos\,(k\pi z/d)\Psi_k(\vec{\rho}), \tag{9}$$

which obeys the boundary condition (4) at the disk sides $z=\pm d/2$ and using the first GL equation (1), one can verify that the longitudinally uniform part of the order parameter $\Psi_0$ gives the main contribution to the expansion (9) for $(\pi\xi/d)^2\gg1$. Therefore, we may assume that the order parameter is uniform along the $z$ direction of the disk and av-

erage the first GL equation over the disk thickness. Since the order parameter does not vary in the $z$ direction, both the superconducting current and the vector potential have no $z$ component. Then the boundary condition (4) is automatically fulfilled at the upper and lower sides of the disk.

In the present paper, we solve the equations for a fixed value of the angular momentum $L$ that leads to the order parameter $\Psi(\vec{\rho})=F(\rho)\exp(iL\phi)$, and consequently both the vector potential and the superconducting current are directed along $\vec{e}_\phi$. In equilibrium the stable $L$ state is the one that minimizes the free energy. The present $L$ states are different from the multivortex state that was studied in Ref. 9. For a fixed angular momentum, Eqs. (6)–(7) can be reduced to the following form:

$$-\frac{1}{\rho}\frac{\partial}{\partial\rho}\rho\frac{\partial F}{\partial\rho}+\left\langle\left(\frac{L}{\rho}-A\right)^2\right\rangle F=F(1-F^2), \tag{10}$$

$$-\kappa^2\left(\frac{\partial}{\partial\rho}\frac{1}{\rho}\frac{\partial\rho A}{\partial\rho}+\frac{\partial^2 A}{\partial z^2}\right)=\left(\frac{L}{\rho}-A\right)F^2\theta(\rho/R)\,\theta(2|z|/d), \tag{11}$$

where we defined the function $\theta(x)=1$ $(x<1)$, and 0 $(x>1)=0$; $\vec{A}=\vec{e}_\phi A$; $R$, $d$ are the dimensionless disk radius and thickness, respectively, and the brackets $\langle\ \rangle$ means averaging over the disk thickness $\langle f(r)\rangle=\int_{-d/2}^{d/2}f(z,r)dz/d$.

The magnetic field created by the superconducting current in the disk has a $H\sim 1/r^3$ dependence similar for a magnetic dipole far away from the disk. Consequently, the condition (5) for the vector potential taken at infinity is transferred to the boundaries of our finite-difference region

$$A(z,\rho=R_s)=\tfrac{1}{2}H_0R_s,\quad A(|z|=d_s,\rho)=\tfrac{1}{2}H_0\rho,$$

where $R_s,d_s\gg R,d$ are the radial and longitudinal sizes of the simulation region. We use typically $R_s,d_s=(5\div 10)\max(d,R)$, where we checked that an increase of the size of the simulation region does not change our results by more than a few percent. The boundary conditions for the order parameter

$$\left.\frac{\partial F}{\partial\rho}\right|_{\rho=R}=0,\quad \left.\rho\frac{\partial F}{\partial\rho}\right|_{\rho=0}=0, \tag{12}$$

correspond to zero current density at the disk surface and a finite value of the first derivative of $F$ at the disk center.

To solve the system of Eqs. (10)–(11) numerically we apply a finite-difference representation on the space grid $\rho_i$, $z_j$. The steady-state solution of the GL equations is obtained using the iteration procedure

$$\begin{aligned}\eta_f F_i^k&-\frac{2}{\rho_{i+1/2}^2-\rho_{i-1/2}^2}\left(\rho_{i+1/2}\frac{F_{i+1}^k-F_i^k}{\rho_{i+1}-\rho_i}-\rho_{i-1/2}\frac{F_i^k-F_{i-1}^k}{\rho_i-\rho_{i-1}}\right)\\&+\left\langle\left(\frac{L}{\rho}-A\right)^2\right\rangle_i F_i^k-F_i^k+3(F_i^{k-1})^2F_i^k\\&=\eta_f F_i^{k-1}+2(F_i^{k-1})^3,\end{aligned} \tag{13}$$

$$\begin{aligned}\eta_a A_{j,i}^k&-\frac{2\kappa^2}{\rho_{i+1/2}-\rho_{i-1/2}}\left(\frac{\rho_{i+1}A_{j,i+1}^k-\rho_iA_{j,i}^k}{\rho_{i+1}^2-\rho_i^2}\right.\\&\left.-\frac{\rho_iA_{j,i}^k-\rho_{i-1}A_{j,i-1}^k}{\rho_i^2-\rho_{i-1}^2}\right)-\frac{2\kappa^2}{z_{j+1/2}-z_{j-1/2}}\left(\frac{A_{j+1,i}^k-A_{j,i}^k}{z_{j+1}-z_j}\right.\\&\left.-\frac{A_{j,i}^k-A_{j-1,i}^k}{z_j-z_{j-1}}\right)-\left(\frac{L}{\rho_i}-A_{j,i}^k\right)F_i^k=\eta_aA_{i,j}^{k-1},\end{aligned} \tag{14}$$

where $A_{j,i}=A(z_j,\rho_i)$, $F_i=F(\rho_i)$, $\rho_{i+1/2}=(\rho_{i+1}+\rho_i)/2$, $z_{j+1/2}=(z_{j+1}+z_j)/2$; the upper index $k$ denotes the iteration step. The introduction of the iteration parameters $\eta_f$ and $\eta_a$ is a well-known procedure in order to speed up the convergency of the iteration procedure. It corresponds to an artificial time relaxation of the system to a steady-state with time steps $1/\eta_f$ and $1/\eta_a$. To further speed up the iteration convergency we expand the nonlinear term $(F_i^k)^3=(F_i^{k-1})^3+3(F_i^{k-1})^2(F_i^k-F_i^{k-1})$ in the right-hand side of the first GL equation. The convergency rate of the above procedure depends strongly on the magnetic-field strength. For typical values of the iteration parameters $\eta_f=2$, $\eta_a=5$, an accuracy of about $10^{-8}$ is reached after a few hundred iteration steps. Near the bifurcation values of a magnetic field corresponding to phase transitions between the superconducting and the normal state, we observe a critical slowing down and the total number of iteration steps that are needed increases by more than an order of magnitude. Since the size of our simulation region exceeds by far those of the disk, we apply nonuniform space grids to diminish the computation time. We took the space grid uniform inside the disk, and increased the grid spacing exponentially with distance outside the disk. This allows us to use almost the same number of grid points inside and outside the disk. We performed calculations with a different number of grid points in order to check that our results are independent of the used space grid.

In general, the nonlinear GL equations have many steady-state solutions. This fact can manifest itself in the experimental observation of hysteresis, when the measured magnetization depends whether one increases or decreases the magnetic field.[4] To mimic those real experimental conditions we perform calculations where the magnetic field is slowly increased from a weak value where the disk is in the superconducting state, or to decrease the field from a large value, where the disk is in the normal state. As an example we consider the latter case. When we reduce the magnetic field below the critical value $H_{nuc}$, which depends on the value of the angular momentum and the disk radius, the normal state becomes unstable and transforms to a superconducting one. The critical magnetic field can be obtained from the linearized first GL equation

$$\hat{L}F=0,\quad \hat{L}=-\frac{1}{\rho}\frac{\partial}{\partial\rho}\rho\frac{\partial}{\partial\rho}+(L/\rho-A_0)^2-1. \tag{15}$$

The superconducting state starts to develop when the minimal eigenvalue of the operator $\hat{L}$ becomes negative. For the zero angular momentum state, the normal state transforms to the superconducting state with decreasing magnetic field below the nucleation field $H_{nuc}$. For nonzero angular momentum, the superconducting state appears when we cross either

the lower $H_{nuc,l}$ or the upper $H_{nuc,u}$ critical magnetic fields that depends on the disk radius. Since our order parameter is represented on a space grid, we find numerically the eigenfunctions and eigenvalues of the operator $\hat{L}$ using the Hounsholder technique. Starting from the critical magnetic fields $H_{nuc,l}$ or $H_{nuc,u}$, we take the initial order parameter to be equal to the lowest eigenfunction. To avoid artificial nonlinear effects that could be produced by the initial condition, we choose a small amplitude for this eigenfunction. The initial vector potential is taken equal to the undisturbed magnetic-field configuration. After finding a steady state, we reduce the applied field by a small value and search for a new solution. Decreasing slowly the magnetic field, we reach its zero value. Increasing the magnetic field, we start either from the lower nucleation field or from the zero magnetic-field value, where the superconducting state can exist for a large disk radius or a small angular momentum.

## III. LINEAR ANALYSIS

The nucleation of the superconducting state can be analyzed using the linearized first GL equation. A knowledge of the eigenvalues of the operator $\hat{L}$ given by Eq. (15) allows one to find the dependence of the nucleation field on the disk radius and the angular momentum. The ground state of the operator $\hat{L}$ was discussed by Moshchalkov and co-workers.[5] To develop a nonlinear approach, which will be considered in the next section, one has to know the whole spectrum and all the eigenfunctions of $\hat{L}$. We will find the excited states of the operator $\hat{L}$ using the Housholder diagonalization technique for our finite-difference representation of $\hat{L}$. In this section, we restrict our discussion to the different ground states that are of interest in the calculation of the nucleation field.

It is known,[10] that the lowest eigenfunctions $\psi_1$ of the operator $\hat{L}$ have the following analytical form:

$$\psi_1=\rho^L \exp\left(-\frac{H_0\rho^2}{4}\right)M\left(-N,L+1,\frac{H_0\rho^2}{2}\right), \qquad (16)$$

where $M(a,c,y)$ is the Kummer function. The eigenfunctions for the angular momenta $L=0,1,2$ are presented in Fig. 2 for four different values of the magnetic flux $\Phi=H_0R^2=0$, 5, 10 and 15 piercing through the disk, measured in units of the flux quantum $\Phi_0=ch/2e$. In the limit of large magnetic flux $\Phi\gg(1+L^2)\Phi_0$ the lowest eigenfunctions approach their asymptotic values $\psi_a=\rho^L \exp(-H_0\rho^2/4)$ that are shown by the dotted curves in Fig. 2 for $\Phi/\Phi_0=10$ and 15 and also for $\Phi/\Phi_0=5$ in the case of $L=0$. The position of the maximum of the order parameter $R_L\sim\sqrt{2L/H_0}$ shifts away from the disk center with increasing angular momentum and decreasing magnetic field.

The lowest eigenvalues of $\hat{L}$ are

$$\lambda_1=\nu_L/R^2-1, \quad \nu_L=\Phi(1+2\nu), \qquad (17)$$

where the value $\nu$ has to be found from the boundary condition (12) at the disk radial boundary, which reduces to the equation

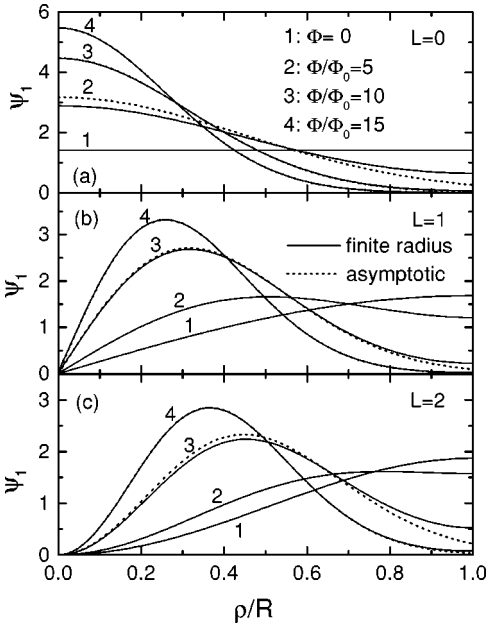


FIG. 2. The lowest eigenfunctions of the linearized first GL equation for different angular momenta $L=0$ (a), $L=1$ (b), $L=2$ (c), and different magnetic flux. The dotted curves show the asymptotic behavior $\psi_1=\rho^L \exp(-H\rho^2/4)$ of the eigenfunctions in the large $\Phi/\Phi_0\gg 1+L^2$ magnetic-flux region.

$$(L-\Phi)M\left(-\nu,L+1,\frac{\Phi}{2}\right)-\frac{2\nu\Phi}{L+1}M\left(-\nu+1,L+2,\frac{\Phi}{2}\right)=0. \qquad (18)$$

The dependencies of $\nu_L$ on the magnetic flux for the ten lowest angular momenta $L=0,1,\ldots,9$ are shown in Fig. 3. For small total magnetic flux the state with zero angular momentum obtains its minimum eigenvalue for zero flux value and the eigenvalue increases with increasing magnetic field. At $\Phi=\Phi_1\approx 1.92\Phi_0$ there is a crossing between the

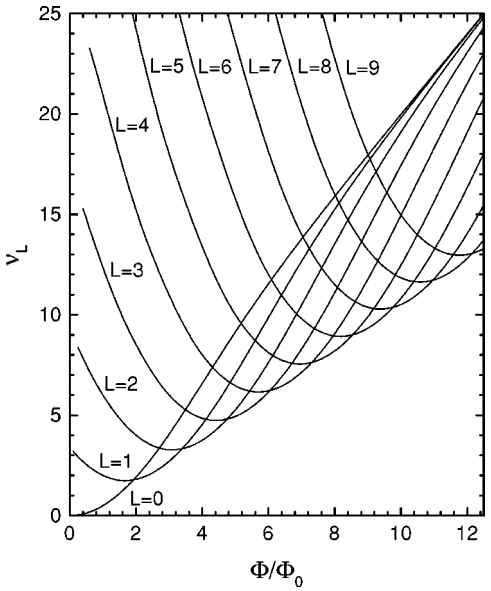


FIG. 3. The magnetic-flux dependency of the lowest eigenvalues of the linearized first GL equation for different angular momenta $L=0,\ldots,9$.

TABLE I. The results of a linear analysis of the first GL equation: $\Phi_L$ is the magnetic flux for switching between the states with angular momenta $L-1$ and $L$; $R_{cr}$ and $\Phi_{cr}$ are the minimum radius for the appearance of the superconducting state and the corresponding magnetic flux, respectively; $H_{nuc}$ is the maximum of the upper nucleation field; $R_{max}$ is the maximum radius corresponding to the appearence of the superconducting state at zero magnetic field.

| $L$ | $\Phi_L/\Phi_0$ | $R_{cr}/\xi$ | $\Phi_{cr}/\Phi_0$ | $H_{nuc,u}/H_{c2}$ | $R_{max}/\xi$ |
|---|---|---|---|---|---|
| 1 | 1.924 | 1.319 | 1.665 | 2.354 | 1.840 |
| 2 | 3.392 | 1.810 | 3.086 | 2.133 | 3.048 |
| 3 | 4.748 | 2.177 | 4.416 | 2.042 | 4.151 |
| 4 | 6.046 | 2.482 | 5.700 | 1.990 | 5.112 |
| 5 | 7.307 | 2.748 | 6.948 | 1.955 | 5.897 |
| 6 | 8.542 | 2.987 | 8.174 | 1.930 | 6.542 |
| 7 | 9.759 | 3.207 | 9.383 | 1.911 | 7.093 |
| 8 | 10.96 | 3.410 | 10.58 | 1.896 | 7.584 |
| 9 | 12.15 | 3.601 | 11.76 | 1.883 | 8.031 |
| 10 | 13.33 | 3.781 | 12.94 | 1.873 | 8.446 |
| 11 | 14.49 | 3.951 | 14.10 | 1.864 | 8.836 |
| 12 | 15.66 | 4.114 | 15.26 | 1.856 | 9.206 |
| 13 | 16.81 | 4.271 | 16.41 | 1.849 | 9.559 |
| 14 | 17.96 | 4.421 | 17.56 | 1.843 | 9.898 |
| 15 | 19.10 | 4.565 | 18.70 | 1.838 | 10.22 |
| 16 | 20.24 | 4.705 | 19.84 | 1.833 | 10.54 |
| 17 | 21.38 | 4.841 | 20.97 | 1.829 | 10.84 |
| 18 | 22.51 | 4.972 | 22.09 | 1.825 | 11.14 |
| 19 | 23.63 | 5.100 | 23.22 | 1.821 | 11.43 |
| 20 | 24.76 | 5.224 | 24.34 | 1.818 | 11.71 |

eigenvalues belonging to the states with $L=0$ and $L=1$. Further increasing the magnetic flux, crossings occur at $\Phi_L$, which are presented in Table I (second column).

Within the linear approximation, the time dependence of the order parameter is described by the following equation:

$$\frac{\partial\psi}{\partial t}=-\lambda_1\psi. \tag{19}$$

Therefore, the state with angular momentum $L$ has the largest increment in time when the flux is in the range $\Phi_L<\Phi<\Phi_{L+1}$, i.e., when $\lambda_1$ is smallest (actually $\lambda_1$ is negative and thus largest in absolute value). For large radius of the disk there is a strong degeneracy of the wave functions in the presence of an uniform magnetic field, and, consequently, all lowest eigenvalues tend to the same limit value $\nu_L \rightarrow \Phi/2\Phi_0$ and $\lambda_1 \rightarrow H_0/H_{c2}-1$ with increasing magnetic flux (see Fig. 3).

The value of the nucleation magnetic field $H_{nuc}$ corresponding to the transition from the normal state to the superconducting state can be found from the condition $\lambda_1=0$. This gives the region of existence of the superconducting states for the different angular momenta that is shown in Fig. 4. For $L=0$ and small disk radius, the superconducting state can exist up to arbitrarily strong magnetic fields as a metastable state. For fixed angular momentum, the value of the nucleation field approaches the bulk critical value $H_{c2}$ for sufficiently large disk radius. Because of surface superconductivity, the superconducting states can appear above $H_{c2}$

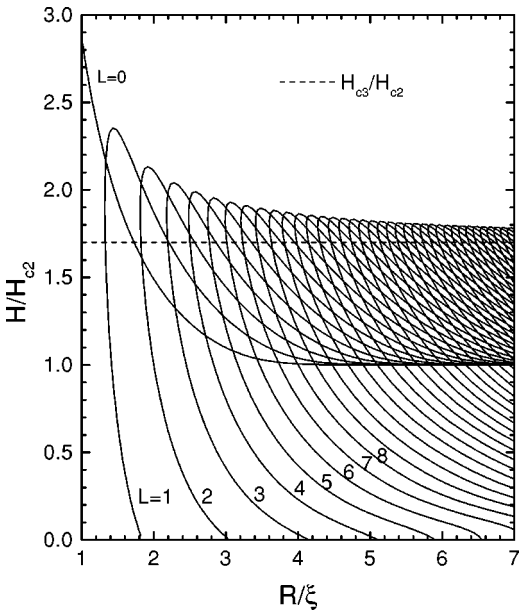


FIG. 4. The nucleation fields as function of the disk radius for different angular momenta $L=0,\ldots,35$. The dotted line corresponds to the nucleation field $H_{c3}\approx 1.7H_{c2}$ for an infinite sample.

even for an arbitrarily large disk. The corresponding magnetic field tends to the value $H_{c3}\approx 1.7H_{c2}$ (Ref. 6) characteristic for surface conductivity of an infinite system. Note, that states with nonzero angular momentum can only exist in sufficiently large samples. The corresponding critical radius $R_{cr}$ and the magnetic flux $\phi_{cr}$ are presented in the third and fourth column of Table I, respectively. Table I gives also the maximum nucleation field (fifth column) and the radius (six column) corresponding to this maximum nucleation field, above which the superconducting state with given angular momentum exists in zero magnetic field. The switching between the states with different angular momentum must be accompanied by jumps in the magnetization. The data presented in Table I allows us to predict the number of those jumps as a function of the disk radius. As an example, Geim *et al.*[4] observed 19 jumps in the magnetization for an aluminum disk with radius 1.2 $\mu$m at the temperature $T=0.4$ K. From Table I we notice that such a number of jumps corresponds to $R/\xi=5.1\div 5.2$ or $\xi\approx 230$ nm, which is in approximate agreement with the estimate of Ref. 4.

## IV. SWITCHING BETWEEN FIRST-ORDER AND SECOND-ORDER PHASE TRANSITIONS

For a given angular momentum, the dimensionless nucleation magnetic field $H_{nuc}$ is completely determined by the radius of the disk. When the penetration length far exceeds the disk size, the magnetic field penetrates unobstructedly into the disk and is practically uniform. In this case, the transition from the superconducting state to the normal state with increasing magnetic field must occur without jumps in the magnetization and the first derivative of the free energy, and is consequently not a first-order transition. Then, the critical magnetic field corresponding to the transition from the superconducting state to the normal state coincides with the nucleation field at the second-order phase transition. When the disk thickness becomes comparable to the penetra-

tion length, the disk exhibits properties characteristic for a type-I superconductor: jumps in the magnetization and a hysteresis behavior. To find the critical disk thickness corresponding to the transition between the different types of behavior, we expand the order parameter over the eigenfunctions of the operator $\hat{L}$. We consider situations where the magnetic field differs weakly from the nucleation field and thus where the order parameter is small.

In order to perform analytical calculations we transform the second GL equation (11) into an integral form

$$A = A_0 + \gamma \hat{G}_0 (L/\rho - A) F^2, \tag{20}$$

with $\gamma = d/\kappa^2$, where the integral operator $\hat{G}_0$ is defined by the relation

$$\hat{G}_0 f = \frac{1}{d} \int_{-d/2}^{d/2} dz_1 \int_0^R d\rho_1 G_0(\rho, \rho_1, z, z_1) \rho_1 f(z_1, \rho_1), \tag{21}$$

with the following kernel[11]

$$G_0(z, z_1, \rho, \rho_1) = \frac{1}{4\pi} \int_0^{2\pi} d\phi \frac{\cos\,\phi}{\sqrt{(z - z_1)^2 + \rho^2 + \rho_1^2 - 2\rho\rho_1 \cos\,(\phi)}}. \tag{22}$$

Keeping terms up to fourth order in $F$, we obtain the following solution to the integral equation (20):

$$A = A_0 + \gamma \hat{G}_0 \eta F^2 - \gamma^2 \hat{G}_0 F^2 \hat{G}_0 \eta F^2, \tag{23}$$

where $\eta = L/\rho - A_0$. This allows us to reduce the system of GL equations to the single integrodifferential equation

$$\hat{L} F = -F^3 + 2\gamma \eta F \hat{G} \eta F^2 - \gamma^2 [2\eta F \hat{G} F^2 \hat{G} \eta F^2 + F(\hat{G} \eta F^2)^2]. \tag{24}$$

In the limit $d \ll \xi$ the vector potential changes weakly inside the disk on the scale of the thickness of the disk. Therefore, to simplify our calculations further we assume that we are allowed to interchange the operations of averaging and integration. The integral operator $\hat{G}$ obtained by averaging $\hat{G}_0$ over the longitudinal coordinate $\hat{G} = \langle \hat{G}_0 \rangle$ has the following kernel:

$$G(\rho, \rho_1) = \frac{1}{4\pi} \frac{1}{d^2} \int_{-d/2}^{d/2} dz \int_{-d/2}^{d/2} dz_1 \int_0^{2\pi} d\phi \times \frac{\cos\,\phi}{\sqrt{(z - z_1)^2 + \rho^2 + \rho_1^2 - 2\rho\rho_1 \cos\,(\phi)}}. \tag{25}$$

As will be shown below, the order of the phase transition is only determined by the first two terms on the right-hand side (RHS) of Eq. (24). Note, that our assumptions $\langle \hat{G}_0 F^2 \hat{G}_0 \eta F^2 \rangle = \hat{G} F^2 \hat{G} \eta F^2$ and $\langle (\hat{G}_0 \eta F^2)^2 \rangle = (\hat{G} \eta F^2)^2$ will not change the critical disk thickness and can only affect the amplitude of the jumps in the order parameter at the first-order phase transition. In the limiting case $d \to 0$, the operator $\hat{G}$ can be expressed[11] in terms of the complete elliptic integrals $K$ and $E$,

$$\hat{G}(\rho, \rho_1) \equiv G_{el}(\rho, \rho_1) = \frac{1}{\pi(\rho_1 + \rho)} \frac{(2 - k^2) K(k) - 2E(k)}{k^2}, \tag{26}$$

with $k^2 = 4\rho\rho_1/(\rho + \rho_1)^2$. Here it is already possible to make some qualitative conclusions about the type of phase transition without solving Eq. (24). The left linear part of Eq. (24) was already discussed in the previous section. When the lowest eigenvalue of the operator $\hat{L}$ becomes negative, the order parameter starts to rise exponentially with time. Therefore, the saturation value of the order parameter is determined by the right part of Eq. (24) containing terms proportional to the cube and fifth power of the order parameter. Note that those terms, which describe the influence of the distortion of the magnetic field, are in fact proportional to powers of $\gamma F^2$ multiplied with $F$. For thin disks ($\gamma \ll 1$), the first term on the RHS of Eq. (24) that suppresses a fast growth of the order parameter is dominant. In this case one would expect a second-order transition between the normal and superconducting states, when the order parameter rises smoothly with increasing deviation of the magnetic field from its nucleation value. In the vicinity of the transition point $|\lambda_1| \ll 1$ the role of higher fifth-order terms are negligible. Since the integral operator $\hat{G}$ is symmetrical and positive definite, the second term on the RHS of Eq. (24) promotes the fast growth of the order parameter. Note, that this term is also proportional to the cubic power of $F$. Increasing the disk thickness, the second term on the RHS of Eq. (24) may become larger than the first one, resulting in the appearance of finite superconductivity for arbitrary small values of $|\lambda_1|$. This indicates the appearance of a first-order phase transition. The value of the order parameter after the transition to the superconducting state is determined by the higher-order terms in Eq. (24).

Next we will give a quantitative treatment of the different phase transitions and solve Eq. (24). In order to do so, we expand the order parameter

$$F = \sum_{k=1}^{\infty} C_k \psi_k, \tag{27}$$

over the eigenfunctions $\psi_k$ of the operator $\hat{L}$, which present a complete basis, each fulfilling the boundary conditions (12). In the neighborhood of the transition point between the superconducting and the normal states the lowest eigenvalue $\lambda_1$ is much smaller than the other eigenvalues $\lambda_{k \neq 1}$. Therefore, the coefficients $C_{k \neq 1}$ are controlled by the amplitude $C_1$ of the leading mode $k = 1$. Keeping terms up to third order in $C_1$, we obtain

$$C_{k \neq 1} = \alpha_k C_1^3, \quad \alpha_k = \frac{1}{\lambda_k} (2\gamma \langle \psi_k \eta \psi_1 | \hat{G} \eta \psi_1^2 \rangle - \langle \psi_k | \psi_1^3 \rangle). \tag{28}$$

Here and below, we use the common definition for the matrix elements

$$\langle f_1|f_2\rangle = \int d\rho f_1(\rho) f_2(\rho)\rho,$$

and the orthogonal basis $\langle \psi_i|\psi_k\rangle = \delta_{ik}$. Note, that in the limit $k \gg 1$ the eigenfunctions $\psi_k$ and eigenvalues $\lambda_k$ are mainly determined by the first term of the operator $\hat{L}$. In this case, the excited states of $\hat{L}$ are close to the usual first-order Bessel functions and the corresponding eigenvalues $\lambda_k$ rise quadratically with the number $k$. Then the coefficients $C_k$ decay quickly with increasing $k$. Substituting expansion (27) into Eq. (25) and keeping terms up to fifth order in $C_1$, we finally derive the equation for the unknown coefficient $C_1$. Since all measured system characteristics are determined by the square of the order parameter, it is more convenient to deal with $C = C_1^2$ that obeys the equation

$$CS(C) = 0, \quad S(C) = -\lambda_1 + BC - AC^2, \tag{29}$$

where

$$B = 2\gamma\langle \eta\psi_1^2|\hat{G}\,\eta\psi_1^2\rangle - \langle \psi_1|\psi_1^3\rangle, \tag{30}$$

and

$$A = 3\Bigg( \gamma^2\langle \psi_1^2|(\hat{G}\,\eta\psi_1)^2\rangle - \sum_{k=2}^{\infty} \frac{1}{\lambda_k}(2\gamma\langle \eta\psi_k|\hat{G}\,\eta\psi_1^2\rangle - \langle \psi_k|\psi_1^3\rangle)^2 \Bigg). \tag{31}$$

Since the operator $\hat{G}$ is positive definite, the first and second terms in the expressions (30) and (31) are positive. As discussed earlier, the sign of the coefficient $B$ controls the type of phase transition that is determined by the competition between two nonlinear effects: (1) the first cubic term on the RHS of Eq. (24) suppresses the growth of the order parameter and gives negative contributions to both coefficients $B$ and $A$; (2) by contrast, the expulsion of the magnetic field from the disk promotes the rise of the order parameter and gives positive contributions to $B$ and $A$.

Equation (29) has three solutions: $C = 0$, which corresponds to the normal state, and

$$C = (B \pm \sqrt{B^2 - 4A\lambda_1})/2A, \tag{32}$$

describing the superconducting state. The time variation of the order parameter obeys the following equation:

$$\frac{dC}{dt} = CS(C)/2. \tag{33}$$

The steady-state solution has to be stable against small perturbations, which gives us the following criterion: $S(C) + CdS(C)/dC < 0$. The normal state ($C = 0$) is stable for $\lambda_1 > 0$. The superconducting state $[S(C) = 0]$ is stable for the plus sign in front of the square root of Eq. (32).

Let us consider the transition from the normal state to the superconducting state, when the eigenvalue $\lambda_1$ changes sign from plus to minus and remains small $|\lambda_1| \ll 1$. The type of transition varies with the sign of the coefficient $B$. For $B < 0$ we are dealing with a second-order transition and the square of the order parameter rises linearly in the vicinity of the nucleation field $C = -\lambda_1/B$. In the other case $B > 0$, we have a first-order transition with a jump in the order parameter. For $A > 0$, the order parameter just after the transition to the superconducting state ($\lambda_1 = 0$) is given by the relation $C = B/A$. For $A < 0$, $B > 0$ we can only predict the existence of a first-order transition. To find the size of the jump in the order parameter one has to take into account higher-order terms in $C$ and thus consider higher-order terms in the expansion (23).

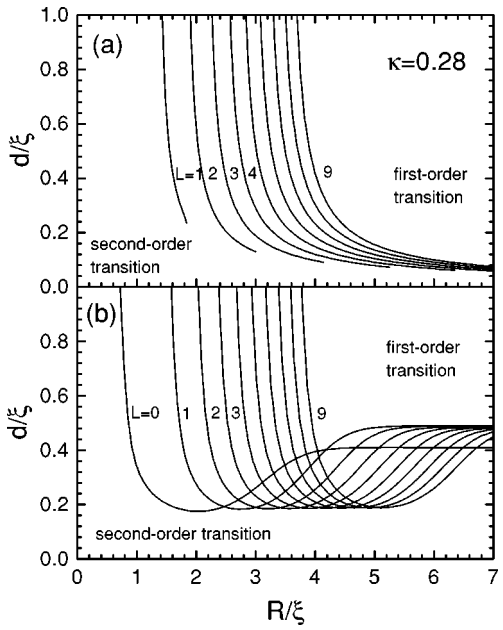


FIG. 5. The critical disk thicknesses as function of the disk radius for the GL parameter $\kappa = 0.28$ and different angular momenta $L = 0, \ldots, 9$ for the lower (a) and upper nucleation fields (b), respectively.

To summarize, the type of phase transition changes with the sign of the coefficient $B$. The corresponding *critical thickness* of the disk

$$d_\star = \frac{\xi\kappa^2}{2} \frac{\langle \psi_1^2|\psi_1^2\rangle}{\langle \eta\psi_1^2|\hat{G}\,\eta\psi_1^2\rangle}, \tag{34}$$

is found from the condition $B = 0$. A second-order transition takes place for $d < d_\star$, while for $d > d_\star$ we have a first-order transition. Equation (34) represents in fact an equation for the unknown $d_\star$ that has to be solved numerically. For $\kappa = 0.28$ and $L = 0, \ldots, 9$ those results are shown in Fig. 5 for the lower (a) and upper (b) nucleation fields, respectively. For $L = 0$ and $R \leqslant \xi$, the critical disk thickness grows rapidly with decreasing disk radius. The same behavior is observed for states with different angular momentum in the vicinity of the critical radius $R_{cr}$ (see Table I) corresponding to the appearance of this state. Whereas the critical thickness decays monotonically with increasing disk radius for the lower nucleation field [see Fig. 5(a)], there is a prominent minimum in the critical thickness for the upper nucleation field [Fig. 5(b)]. Note, that this minimum critical thickness $d_{min}$ changes very weakly with the angular momentum that is reached at $R_{min}$. We were able to obtain the following fitting expressions for the minimum radius:

$$R_{min}/\xi \approx 1.983 + 0.577\kappa^2, \quad L = 0, \tag{35}$$

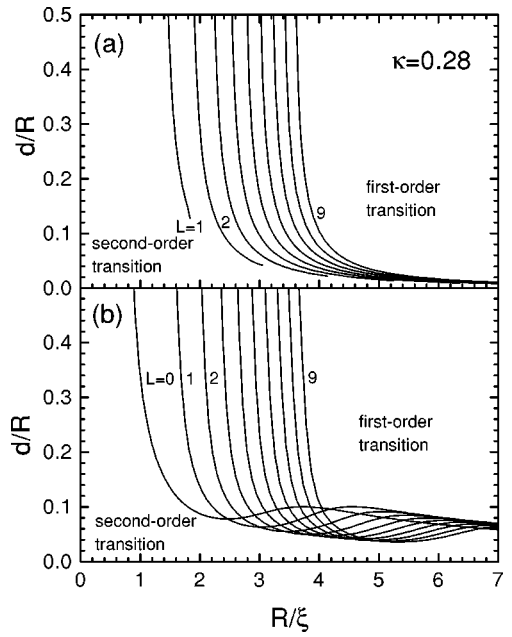


FIG. 6. The ratio between the critical disk thickness and the disk radius versus disk radius for the GL parameter $\kappa=0.28$ and different angular momenta $L=0,\ldots,9$ for the lower (a) and upper nucleation fields (b), respectively.

$$R_{min}/\xi \approx 1.535+0.379\kappa^2+1.175\sqrt{L}, \quad L\neq 0,$$

and the minimum thickness

$$d_{min}/\xi\kappa^2 \approx 2.049+2.397\kappa^2, \quad L=0, \tag{36}$$

$$d_{min}/\xi\kappa^2 \approx 2.145L^{0.016}+2.384\kappa^2 L^{-0.013}, \quad L\neq 0,$$

for arbitrary $\kappa$ and consequently for different materials with an accuracy of about 0.5% in the range $L=0\div 9$.

For a large disk radius $R\gg\sqrt{1+L^2}$ the critical thickness approaches its asymptotic value $d_{as}$ which is independent of $R$. We found numerically the following asymptotes:

$$d_{as}/\xi\kappa^2=4.237+12.72\kappa^2, \quad L=0, \tag{37}$$

$$d_{as}/\xi\kappa^2=4.783+18.83\kappa^2, \quad L\neq 0,$$

with an accuracy of about 2%. The limit of the large disk radius corresponds in fact to the case of thin films. From Eq. (37) we make the important observation that *the phase transition between the superconducting and the normal state of a thin* $(d/\xi<1)$ *type*-II $(\kappa>1/\sqrt{2})$ *superconductor film is always a second-order transition.*

There are two ways to observe the transition between the different behaviors of mesoscopic disks. First, one can prepare disks with different sizes. Second, which is a more elegant way, is to observe transitions between the superconducting and the normal states for the same disk at different temperatures. In this case, the ratio $d/R$ remains constant while $R/\xi\sim(1-T/T_0)^{1/2}$ decreases with increasing temperature. For this purpose we transform Fig. 5 into Fig. 6, where we plot the ratio of the critical thicknesses to the radius of the disk as a function of $R/\xi$ for $\kappa=0.28$ and $L=0,\ldots,9$. As is evident from Fig. 6, increasing the sample temperature, i.e., decreasing $R/\xi\sim(1-T/T_0)^{1/2}$, one can go from a first-order to a second-order phase transition. Such a behavior was observed in the experiments by Geim *et al.*[4] on an Al disk with a thickness of $d=0.15$ $\mu$m and a radius of $R=0.5$ $\mu$m, i.e., $d/R=0.3$, which for $T=0.4$ K ($R/\xi\approx 1.7$ with $\xi(0)=250$ nm) exhibited a first-order superconductor to normal transition that for $T=0.92$ K (i.e., $R/\xi\approx 1$) was a second-order transition that is consistent with Fig. 6.

Next we will try to find an analytical expression for the critical thickness $d_\star$ [Eq. (34)] at which the system goes from a type-II behavior $(d<d_\star)$ to a type-I behavior $(d>d_\star)$. First we notice that the kernel of the integral operator $\hat{G}$ decreases weakly with the disk thickness. In the limit $\kappa\to 0$ the critical disk thickness is proportional to $\kappa^2$,

$$d_\star=\frac{\xi\kappa^2}{2}\int_0^R \psi_1^4(\rho)\rho d\rho\left(\int_0^R \eta(\rho)\psi_1(\rho)^2\rho d\rho \times\int_0^R G_{el}(\rho,\rho_1)\,\eta(\rho_1)\psi_1(\rho_1)^2\rho_1 d\rho_1\right)^{-1}, \tag{38}$$

and therefore $d_\star$ in terms of $\xi\kappa^2$ increases slowly with the GL parameter $\kappa$. We were able to obtain the following fitting expressions for the critical disk thickness:

$$d_\star/d_{min}=2-d_{as}/d_{min} +2\frac{d_{as}/d_{min}-1}{1+\exp\left[-0.818(R-R_{min})^2/\xi^2\right]}, \quad R>R_{min} \tag{39}$$

$$d_\star/d_{min}=1+a\frac{(R-R_{min})^2}{\xi^2} \times\exp\left(b(1+c\kappa^2)\frac{(R-R_{min})^2}{\xi^2}\right), \quad R<R_{min},$$

with $a=0.254$, $b=0.7$, $c=10$ for $L=0$, and $a=0.403-0.029L$, $b=1.1$, $c=4$ for $L\neq 0$. From these expressions one can estimate the critical thickness of the disk for different materials and disk radii with an accuracy of about 6% in the interesting range $d_\star/\xi<1$ and $\kappa\leqslant 0.42$. Note, that for large $\kappa>0.4$ and $d>d_\star$ the main assumption of our analysis: $(d/\pi\xi)^2\ll 1$ breaks down and one has to consider the full 3D problem where the order parameter changes not only in the radial direction but also in the longitudinal one.

Therefore, we also solved the full GL equations numerically using our finite-difference method for mesoscopic disks with different radius and thickness (still in the limit $d\ll\xi$). Figure 7 shows the dimensionless magnetization

$$M=\frac{1}{4\pi V H_{c2}}\int H_s d\vec{r}, \tag{40}$$

for disks with $R/\xi=0.5,\ 1,\ 1.5,\ 2$ in the case of $\kappa=0.28$. The volume integration in Eq. (40) is performed over the disk region, where $H_s$ is the $z$ component of the magnetic field created by the superconducting currents in the disk. In Fig. 7 we give the results of our full 3D calculation (solid curve) and the results from the above expansion (dotted

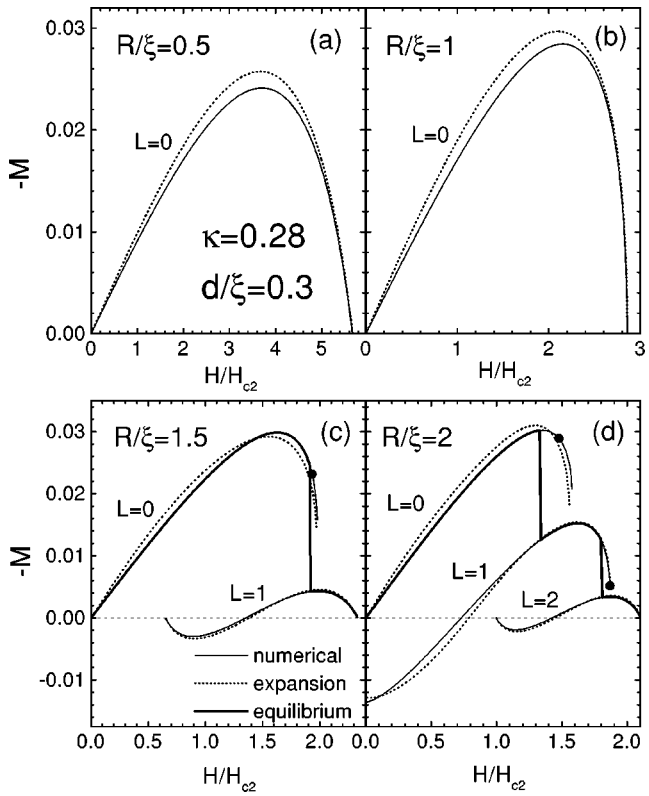


FIG. 7. The magnetic-field dependence of the disk magnetization in disks with $d/\xi=0.3$, $\kappa=0.28$, $R/\xi=0.5$ (a), $R/\xi=1$ (b), $R/\xi=1.5$ (c), $R/\xi=2.0$ (d) for different allowed angular momenta in the case of increasing magnetic field. The dotted and thick curves correspond to results of our approximate approach and the equilibrium state, respectively. The position of the jump in the magnetization for decreasing magnetic field are shown by solid circles for the upper nucleation field in the case, when there is a hysteresis behavior.

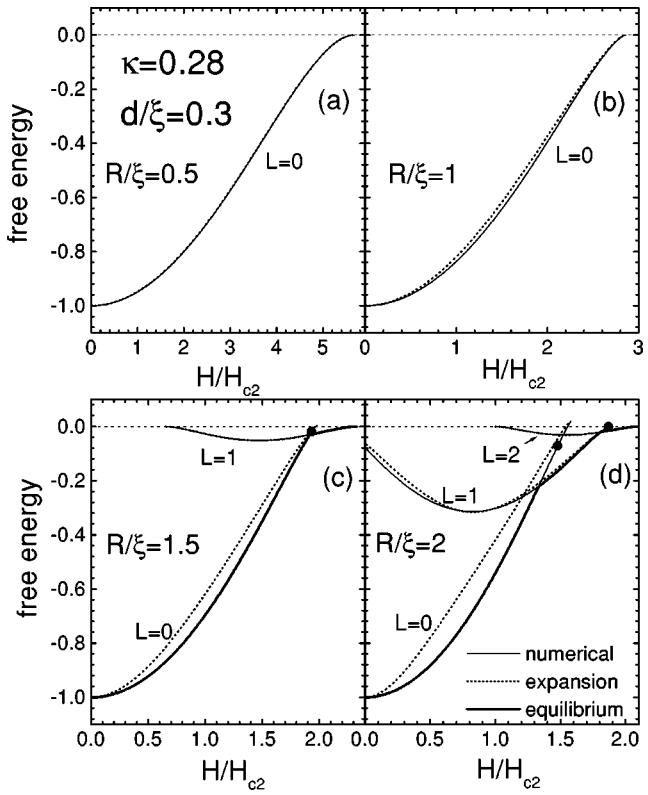


FIG. 8. The Gibbs free energy as function of the magnetic field in disks with $d/\xi=0.3$, $\kappa=0.28$, $R/\xi=0.5$ (a), $R/\xi=1$ (b), $R/\xi=1.5$ (c), $R/\xi=2.0$ (d) for different allowed angular momenta in the case of increasing magnetic field. The dotted and thick curves correspond to results of our approximate approach and the equilibrium state, respectively. The free energies for decreasing magnetic field are shown by solid circles for the upper nucleation fields in the case, when there is a hysteresis behavior.

curve). The thick solid curve presents the magnetization in the lowest energy state. For the considered disk thickness $d/\xi=0.3$ the critical value of the disk radius corresponding to switching between the first-order and the second-order phase transitions are $R/\xi\approx 1.08,\ 1.94,\ 2.40$ for $L=0,1,2$, respectively. Therefore, the transition from the superconducting to the normal state is not accompanied by a jump in the magnetization when $R/\xi=0.5,1$. Note, that near the critical radius [Fig. 7(b)] the magnetization has a large slope at the transition to the normal state. On the other hand, if the disk radius is just above the critical one [see Fig. 7(d)], there is a jump in the magnetization that is rather small in the case of $R/\xi=2$ and $L=1$.

The free energy of the superconducting states corresponding to the different angular momenta are shown in Fig. 8 for $d/\xi=0.3$, $\kappa=0.28$, and $R/\xi=0.5,1,1.5,2$. The magnetic-field dependence of the free energy is similar to the one of the eigenvalues $\nu_L$ (see Fig. 3). Notice that the zero angular momentum state [Fig. 8(a)] has a dimensionless free energy of $-1$ at $H=0$ that corresponds to the condensation energy at zero magnetic field. The equilibrium of the system corresponds to the state with minimum Gibbs free energy (thick curves in Fig. 8) that gives us the rule of switching between states with different angular momentum. Due to the expulsion of the magnetic field from the disk (see Figs. 9 and 10) this switching happens at values of the total magnetic flux that are larger than those obtained from a linear analysis. For example, switching between the states with $L=0$ and $L=1$ occurs at $\Phi/\Phi_0\approx 2.16,2.66$ for $R/\xi=1.5,2.0$, whereas the above linear approach gives $\Phi_1/\Phi_0=1.92$. For second-order phase transitions the Gibbs free energy increases monotonically with magnetic field and becomes zero in the transition point. For first-order transitions, the free energy is positive just before the transition to the normal state and this superconducting state is not energetically favorable and consequently a transition to a different angular momentum state occurs in equilibrium before the transition to the normal state. It should be stressed that experimental observations showing a hysteresis behavior for the magnetization may indicate that the system stays in a definite metastable $L$ state without following the minimum energy curve. Magnetization of the superconducting equilibrium state is shown in Fig. 7 by the thick curves in the cases (c,d) when states with nonzero angular momentum can have lower energy (see Fig. 8). Note, that as a function of the magnetic field the system with a fixed nonzero angular momentum exhibits either diamagnetic or paramagnetic behavior. We found that the region of paramagnetic behavior is energetically unfavorable (see Fig. 8). Previously, other theoretical works[5,12] have addressed the possible origins of paramagnetic superconducting behavior.

The radial distribution of the order parameter (a) and the

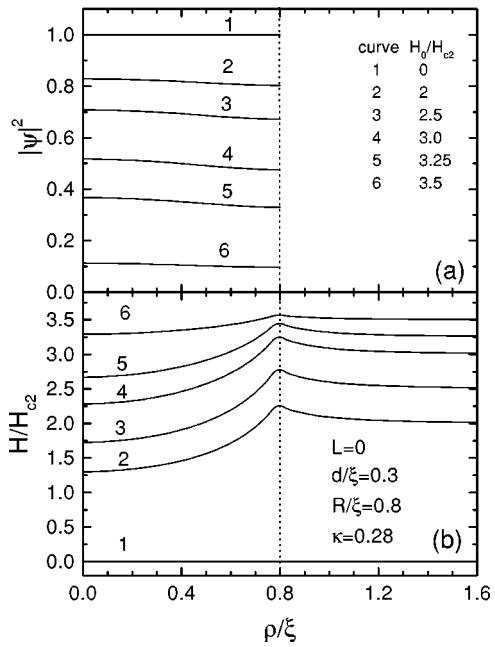


FIG. 9. The spatial distribution of the square of the order parameter (a) and the magnetic field (b) in a disk with $d/\xi=0.3$, $\kappa=0.28$, $R/\xi=0.8$ (a) for different applied magnetic fields.

magnetic field (b) for $d/\xi=0.3$, $\kappa=0.28$ are depicted in Figs. 9 and 10 for two different disk radii $R/\xi=0.8$ and $R/\xi=2$, respectively. For the system with the smaller disk radius $R/\xi=0.8$, we have a second-order phase transition. The order parameter changes rather weakly with distance from the disk center and exhibits an overall decrease with increasing field. The total magnetic flux through the disk and in the surrounding region should be constant (see Fig. 1). Therefore, expulsion of the magnetic field from the disk leads to its enhancement at the disk boundary and the surrounding

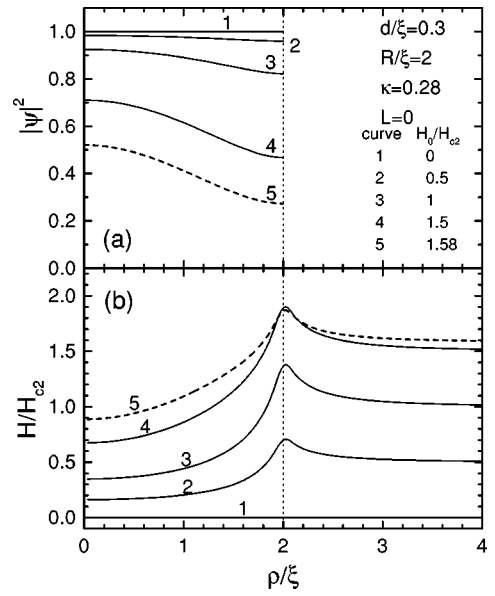


FIG. 10. The spatial distribution of the square of the order parameter (a) and the magnetic field (b) in disks with $d/\xi=0.3$, $\kappa=0.28$, $R/\xi=2.0$ (a) for different applied magnetic fields. The dashed curves correspond to the superconducting state just before the first-order transition to the normal state.

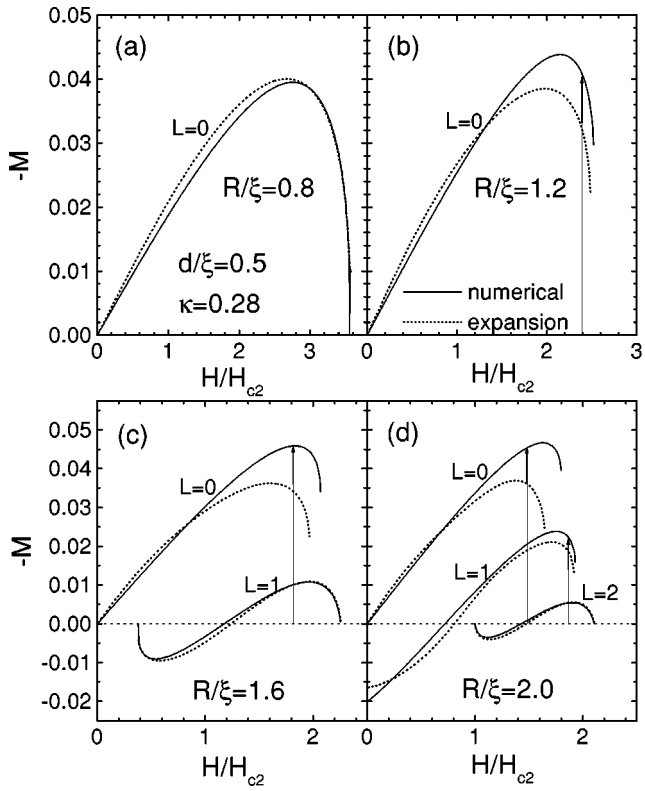


FIG. 11. The magnetization as function of increasing magnetic field for disks with $d/\xi=0.5$, $\kappa=0.28$, $R/\xi=0.8$ (a), $R/\xi=1.2$ (b), $R/\xi=1.6$ (c), $R/\xi=2.0$ (d) and for different allowed angular momenta. The dotted curves correspond to results of our approximate approach. The vertical arrows show transitions from the normal state to the superconducting state in the case of decreasing magnetic field.

insulator media (see Fig. 9). For $R/\xi=2$ the $L=0$ state exhibits a first-order transition. In this case, the order parameter remains finite just before the transition to the normal state that occurs at $H/H_{c2}\approx 1.58$. Note also that the order parameter decreases much more near the disk boundary as compared to the smaller disk (Fig. 9). Similar results for the magnetization are shown in Fig. 11 for thicker disks. Note that these thicker disks (see Fig. 11) show a similar pattern of phase transitions that are qualitatively not different from the small disk radius case. But the hysteresis is more prominent for thicker disks. The critical field for transition to the normal state is larger than the nucleation field depicted by the vertical arrows in Fig. 11.

## V. SYSTEM CHARACTERISTICS AT THE FIRST-ORDER TRANSITION

In the immediate vicinity of the transition point $|\lambda|\ll 1$, the order parameter of the superconducting state is given by the relation (32) with a plus sign in front of the square root. At the point where the system transforms from the normal state to the superconducting state, we have $\lambda_1=0$ at the nucleation field and the order parameter equals $C_n=B/A$. In the reverse direction, when there is a transition from the superconducting state to the normal one, the solution of Eq. (29) still exists for $\lambda<\lambda_\star=B^2/4A$. Note, that we consider analytically only the case $A>0$, where our expansion is

valid. The order parameter before the transition to the normal state is $C_t = B/2A$, which is two times smaller than $C_n$. Since our expansion is essentially based on the assumption $C \ll 1$, analytical results are valid only in the vicinity of small $B$. Consequently, the value of the magnetic field $H_t$ corresponding to a transition to the normal state differs weakly from the nucleation field $H_n$, which allows us to use the following expansion for the lowest eigenvalue:

$$\lambda(H_t) = a_\lambda (H_t - H_n), \quad a_\lambda = -\langle \psi_1 | \rho \eta \psi_1 \rangle, \tag{41}$$

from which we find analytically the critical field

$$H_t = H_n + \frac{B^2}{4 a_\lambda A}. \tag{42}$$

Note, that $H_t > H_{nuc,t}$ and $H_t < H_{nuc,l}$. Substituting expansion (27) into Eq. (8) we obtain a compact expression for the Gibbs free energy at the nucleation point $F_n$ and just before the transition to the normal state $F_t$,

$$F_n = -\frac{2B^3}{3A^2R^2}, \quad F_t = \frac{B^3}{6A^2R^2}. \tag{43}$$

Note, that the superconducting state before the first-order transition to the normal state is always metastable $F_t > 0$. The absolute values of $F_n$ is four times larger than $F_t$. Magnetization at the nucleation point $M_n$ and before switching to the normal state $M_t$ have the same sign and differ by a factor of 2 in absolute value,

$$M_n = \frac{\gamma B}{2\pi A R} \int_0^R d\rho G_{el}(R,\rho)\, \eta \psi_1^2, \quad M_t = \tfrac{1}{2} M_n. \tag{44}$$

Here we took only the first term of the expansion of $M_n, M_t$ in the square of the order parameter $C$.

The results of our numerical solution of the GL equations (solid curves) are presented in Figs. 12, 13, and 14 that confirm the above analysis (dotted curves) in the range of validity of our expansion $B \ll A$. Figures 12 and 13 show the values of $H_n$, $H_t$ (a); $F_n$, $F_t$ (b); $M_n$, $M_t$ (c) for the upper nucleation field at $d/\xi = 0.3$, $\kappa = 0.28$ and for different angular momenta $L = 0$ (Fig. 12) and $L = 2$ (Fig. 13). The same characteristics are presented in Fig. 14 for the lower nucleation field for $L = 2$. Note, that for the upper nucleation field the system exhibits the usual diamagnetic response that grows with increasing disk thickness and with decreasing GL parameter $\kappa$, whereas there is a *paramagnetic Meissner effect* for lower nucleation fields. The critical field $H_t$, obtained from a full numerical solution of the GL equations, is shown in Fig. 15 for different thicknesses of the superconducting disk and for three angular momenta $L = 0,1,2$. The hysteresis behavior that can be characterized by the difference $|H_t - H_n|$ becomes more prominent with increasing disk thickness, as expected. Note, that there are maxima in the dependencies of $|H_t - H_n|$ on the disk radius, which coincides approximately with the minima of the critical disk thicknesses presented in Fig. 5. According to our analytical predictions, the hysteresis in the magnetic field disappears with increasing disk radius for relative small disk thicknesses. As seen from Fig. 5, the region of first-order transitions, i.e., $B > 0$, is obtained for a disk thickness of $d/\xi = 0.3$ restricted to the disk radius with $R_l < R < R_u$ where a first-order transition takes place. The system should exhibit a second-order transition for $R > R_u \approx 3.2, 3.8, 4.2\xi$ for $L = 0,1,2$. Note that the size of the jumps in the free energy and in the magnetization approach zero when the disk radius reaches the lower boundary $R_l$. On the other hand, when the disk radius approaches the upper limit $R_u$ there are still jumps that indicate a *new type of phase transition.*

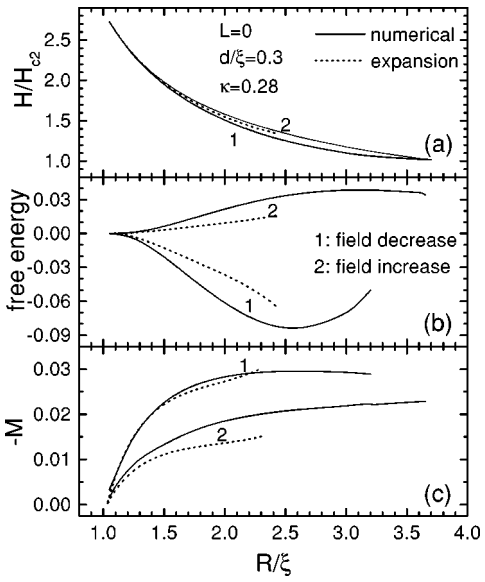


FIG. 12. The critical magnetic field (a) corresponding to the transition between the superconducting and the normal state, the Gibbs free energies (b), and magnetizations (c) just after the transition for decreasing (1) and increasing (2) magnetic field. The GL parameter $\kappa = 0.28$ and $L = 0$. The dotted curves depict the results of our analytical approach.

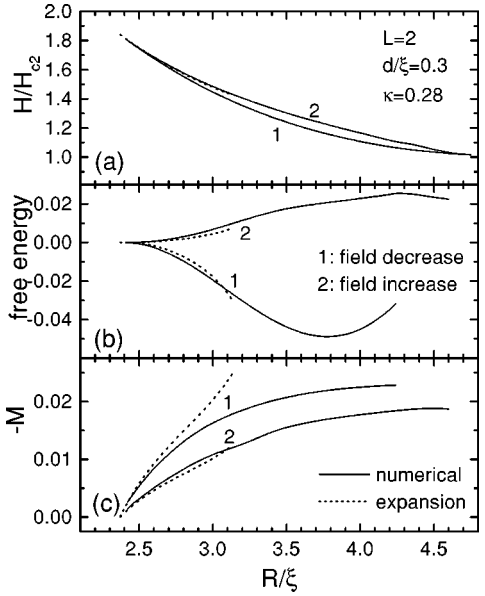


FIG. 13. The critical magnetic field (a) corresponding to the transition between the superconducting and the normal state for the upper nucleation field, the Gibbs free energies (b), and magnetizations (c) just after the transition for decreasing (1) and increasing (2) magnetic field for $\kappa = 0.28$, $L = 2$. The dotted curves depict the results of our analytical approach.

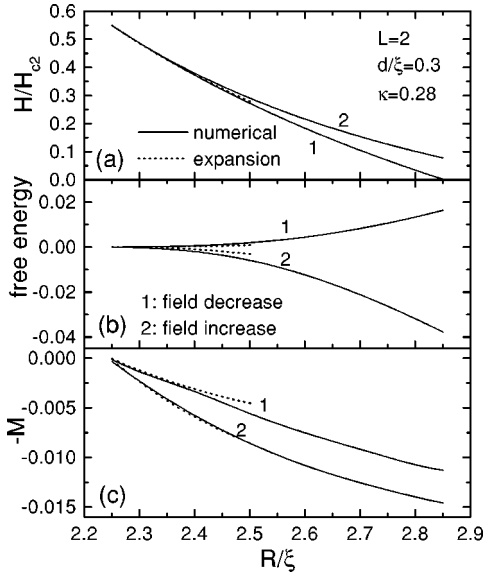


FIG. 14. The critical magnetic field (a) corresponding to the transition between the superconducting and the normal state for the lower nucleation field, the Gibbs free energies (b), and magnetizations (c) just after the transition for decreasing (1) and increasing (2) magnetic fields at $\kappa=0.28$, $L=2$. The dotted curves depict the results of our analytical approach.

Strictly speaking, our analytical approach is only valid in the vicinity of the nucleation field. However, it turns out that the above approach allows us to predict free energies and magnetizations in the whole region of magnetic fields with a good accuracy for the relatively small, i.e., $R \leqslant R_{min}$, radii of the disk. Substituting expansion (27) in Eq. (8) we can write the relation for the Gibbs free energy in the following form:

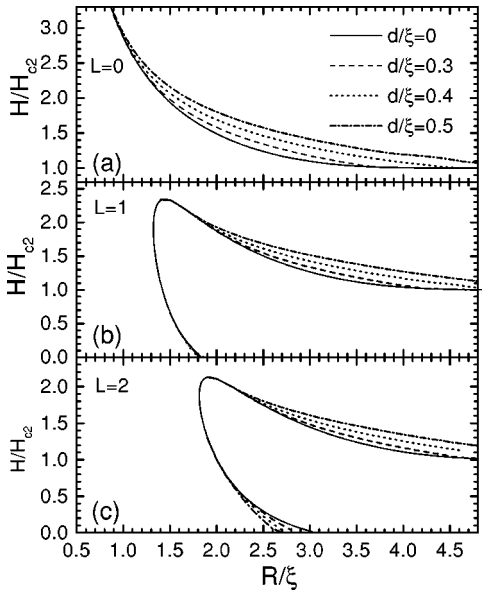


FIG. 15. The critical magnetic field (a) corresponding to the transition between the superconducting and the normal state for $\kappa=0.28$ and the different angular momenta $L=0$ (a), $L=1$ (b), $L=2$ (c). The solid curves show the nucleation field. Other curves depict the values of the critical magnetic field for the different disk thicknesses in the case when the system goes from the superconducting state to the normal state.

$$F=\frac{2}{3}\frac{C}{R^2}(4\lambda_1-BC), \tag{45}$$

where the square of the order parameter $C$ is given by Eq. (32) with the plus sign in front of the square root. In order to find the magnetization of the disk one has to solve Eq. (20). The use of an infinite series instead of expansion (23) could encounter some obstacles due to convergency of such series for a finite value of the order parameter, when the maximum eigenvalue of the operator $2\gamma\hat{G}\eta F^2$ is larger than unity. To avoid this problem we applied the following trick. Rearranging the main term with the vector potential from the RHS to the left-hand side of Eq. (20) and keeping terms up to second order in $C$, we rewrite Eq. (20) in the following form:

$$(1+C\gamma\hat{G}\psi_1^2)A_s=\gamma\hat{G}\eta F^2. \tag{46}$$

Here $A_s=A-A_0$ is the vector potential created by the superconducting currents in the disk. In spite of these simplifications, Eq. (46) represents in fact an integral equation, which has to be solved numerically. The magnetization of the disk given by Eq. (40) can be expressed in terms of the vector potential $A_t=A_s(\rho=R)$ at the disk boundary $M=A_t/2\pi R$. Therefore, we have only to calculate $A_t$. Assuming an uniform field distribution over the disk $A_s=\rho A_t/R$, we can solve Eq. (46) for the unknown coefficient $A_t$ and represent finally the magnetization

$$M=\frac{\gamma C}{2\pi R}\left[\int_0^R d\rho G(R,\rho)\eta\rho\psi_1\left(\psi_1+C\sum_{k=2}^{\infty}\alpha_k\psi_k\right)\right]\times\left(1+\frac{\gamma C}{R}\int_0^R d\rho G(\rho,R)\rho^2\psi_1^2\right)^{-1}, \tag{47}$$

in terms of integrals over the disk, where the coefficients $\alpha_k$ are given by Eq. (28). The results obtained by using Eqs. (45) and (47), which are shown in Figs. 7, 8, and 11 by the dotted curves for $d/\xi=0.3$ and 0.5 and for different radius of the disk, correlate well with our numerical results for small radius and large angular momentum. This implies that we are allowed to use Eqs. (45) and (47) in order to estimate the magnetization of small disks.

## VI. PHASE TRANSITION IN LARGE RADIUS DISKS

Large radius disks show new features in their phase transition behavior that cannot be explained in the above simple model where only the sign of the coefficient $B$ at the nucleation point was considered. This is illustrated in Figs. 16 and 17 where the free energy and magnetization are shown for disks with $R/\xi=3.5$, $\kappa=0.28$ and two different thicknesses $d/\xi=0.18$ (Fig. 16) and $d/\xi=0.3$ (Fig. 17). The disk with $d/\xi=0.18$, is thinner than the critical thickness for all angular momenta in the case of the upper nucleation field [see Fig. 5(b)], and therefore exhibits a second-order reversible transition between the superconducting and the normal state for increasing magnetic field. As seen from Fig. 5(a), the critical thickness for the superconducting state with $L=3$ is smaller than $0.18\xi$ for the lower nucleation field. Indeed, our numerical solution of the full GL equations shows a first-order transition for this state (dotted curves in Fig. 16) in low

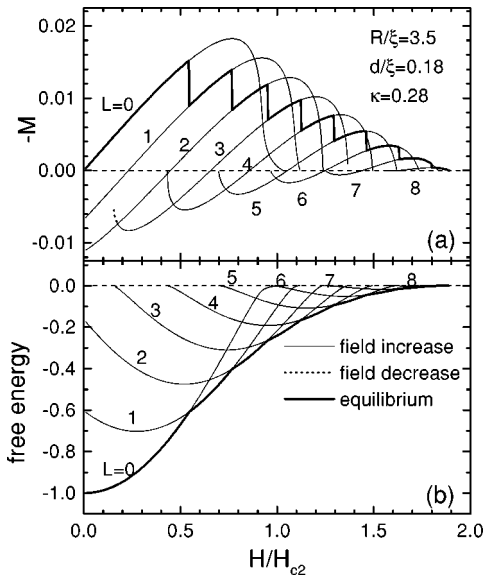


FIG. 16. Magnetization (a) and the Gibbs free energy (b) of states with different angular momenta $L=0,\ldots,8$ as a function of the magnetic field for $d=0.18\xi$, $R=3.6\xi$, $\kappa=0.28$. Thin and dotted curves correspond to increasing and decreasing magnetic fields, respectively. Thick curves correspond to the equilibrium state for which the free energy is minimal.

magnetic field. For the thicker disk $d/\xi=0.3$ and if we consider the upper nucleation field, the phase transition should be second order for the zero angular momentum state and first order for the other momenta. For the lower nucleation

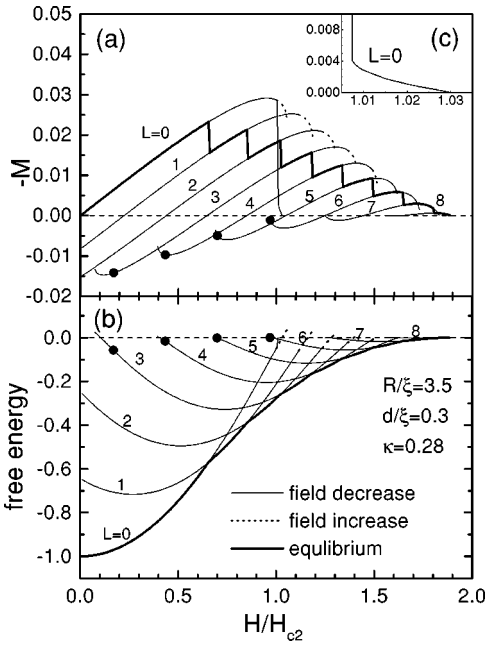


FIG. 17. The dependencies of the disk magnetization (a) and the Gibbs free energy (b) on the magnetic field for a disk with $d/\xi=0.3\xi$, $\kappa=0.28$, $R/\xi=3.5$ (a). Thin and dotted curves correspond to increasing and decreasing magnetic fields, respectively. Thick curves correspond to the equilibrium state with a minimum of free energy. Inset (c) shows magnetization of the disk for the superconducting state with zero angular momentum in decreasing magnetic field.

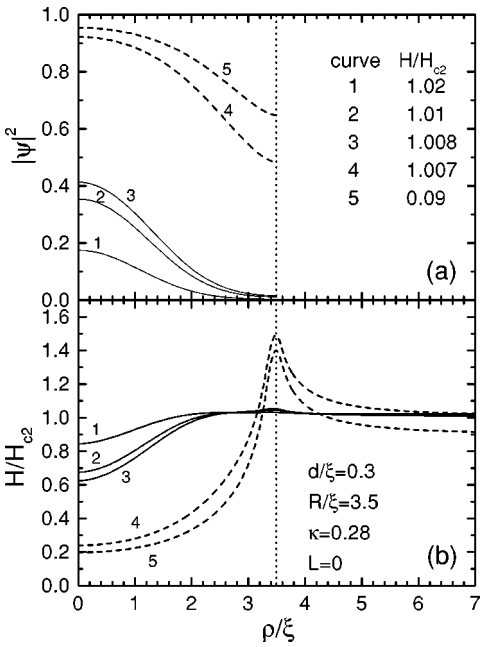


FIG. 18. The spatial distribution of the square of the order parameter (a) and the magnetic field (b) for $d/\xi=0.3$, $\kappa=0.28$, $R/\xi=3.5$, $L=0$, and different applied magnetic fields. Solid and dotted curves correspond to superconducting states before and after the first-order transition shown in Fig. 17(c), respectively.

field, first-order transitions should be observed for $L=3,4,5,6$. The results of our numerical calculation confirm these predictions for the case of decreasing magnetic field, when the system goes from the superconducting state to the normal state (see Fig. 17). When the magnetic field increases from its zero value, there are jumps in the free energy and the magnetization even for the zero angular momentum state. This situation cannot be described in the framework developed in the previous section, where only weak distortions of the magnetic field were allowed in our quasilinear approach. For the present large radius disks large distortions of the magnetic field near the superconducting disk boundary are possible at the transition to the normal state. More interesting behavior of the magnetization is shown in Fig. 17(c) [inset of Fig. 17(a)] for the $L=0$ state. In accordance to the prediction of the analytical approach, there is a second-order phase transition at the nucleation point. But further decreasing the magnetic field leads to a first-order transition to another superconducting state. Figure 18 presents the radial distribution of the order parameter and the magnetic field for this case $d/\xi=0.3$, $R/\xi=3.5$, $\kappa=0.28$, $L=0$. As seen from Fig. 18, there is a rather large distortion of the magnetic field just before the transition (compare curves 3 and 4 that are for $H/H_{c2}=1.008$ and 1.007, respectively), which is the reason why our previous analytical approach could not be applied. Note that at this phase transition the contribution of surface conductivity at the perimeter of the disk to the superconducting state changes in a discontinuous way. This is further illustrated in Fig. 19 where the magnetic-field dependence of the magnetization is shown for different disk radii for the zero angular momentum state and $d/\xi=0.3$, $\kappa=0.28$. As is evident from Fig. 19, a first-order transition between the different superconducting states occurs in both cases—of decreasing and increasing magnetic field. Note, that the ampli-

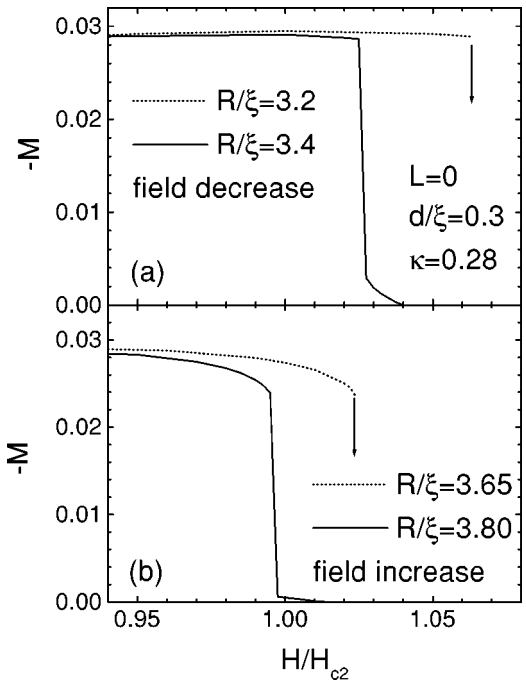


FIG. 19. Magnetization of a disk in decreasing (a) and increasing (b) magnetic field for $d/\xi=0.3$, $\kappa=0.28$, zero angular momentum and different disk radii.

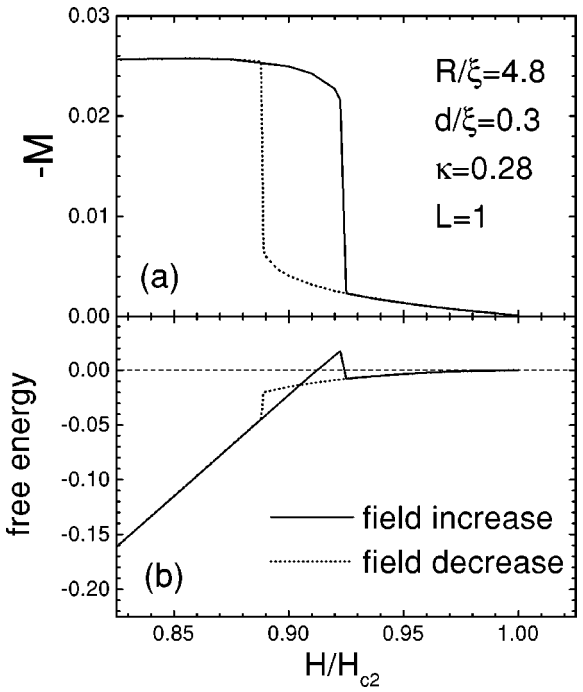


FIG. 20. Magnetization of the disk in decreasing (dotted curves) and increasing (solid curves) magnetic field for $d/\xi=0.3$, $\kappa=0.28$, $L=0$, $R/\xi=4.8$.

tude of the jumps in the magnetization weakly changes with the disk radius and coincides with the data presented in Fig. 12. Thus, when the disk radius increases and the value of the coefficients $B$ becomes negative, we are dealing with a first-order transition between two superconducting states. Figure 20 shows, that this type of behavior is not peculiar to the state with zero-angular momentum.

To understand the physical reason for the appearance of a first-order transition between two superconducting states we return to our analytical approach. As noted above, the sign of the coefficients $B$ and $A$ at the transition point depends on the disk size and the value of the GL parameter $\kappa$. The four possible cases are shown in Fig. 21 for $L=0,1,2$ and $\kappa=0.28$. The regimes I ($B<0$, $A>0$) and II ($B>0$, $A>0$) correspond to second-order and first-order transitions between the superconducting and the normal states, respectively, and have been discussed in the previous section. Now the case $A<0$ is of interest to us. When the disk thickness is larger than the critical thickness and $B>0$, we are dealing with a first-order transition. For $A<0$, the above analytical approach does not allow us to predict the amplitude of the jumps in the magnetization and the free energy since higher-order terms in the expansion have to be included. Crossing the boundary between regions III ($B>0$, $A<0$) and IV ($B<0$, $A<0$), we can apply our approach once again in the vicinity of the point $B=0$. For small negative $B$ a second-order transition takes place at the nucleation field. While the order parameter $C\sim\lambda$ remains rather small, the condition $B-AC<0$ is fulfilled and the superconducting state is stable relative to weak perturbations. Since the coefficient $A$ is negative in the region IV, the situation changes radically with further decreasing of the magnetic field. For some critical value of the magnetic field $H_s$, the expression under the square root in Eq. (32) becomes negative. This means an instability of the system and its transition to another state. Unfortunately, we cannot predict the characteristics of this new state. But the relation $\lambda_1=B^2/A$ allows us to find the critical magnetic field $H_s$ just as we did for the field $H_t$ (42). Nearby the boundary between the regions III and IV, the value of $H_s$ calculated from the above approach correlate well with the numerical results for $L=1,2$ as presented in Fig. 22. For zero-angular momentum and $d/\xi=0.3$ we have a more complicated situation, because crossing the boundary

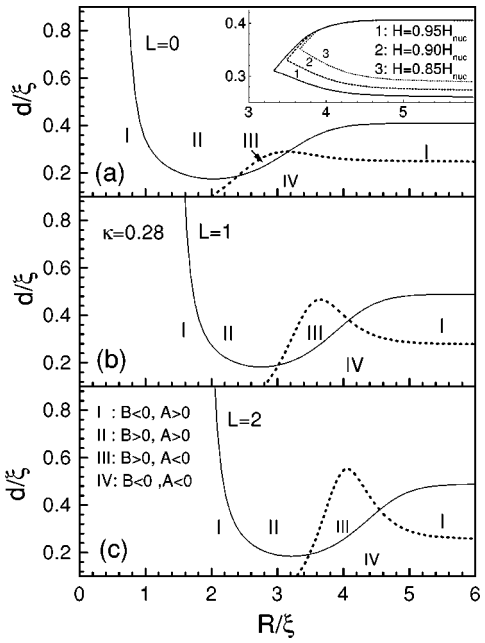


FIG. 21. The phase diagram classifying the regions of different types of phase transitions for $\kappa=0.28$ and the different angular momenta $L=0$ (a), $L=1$ (b), $L=2$ (c).

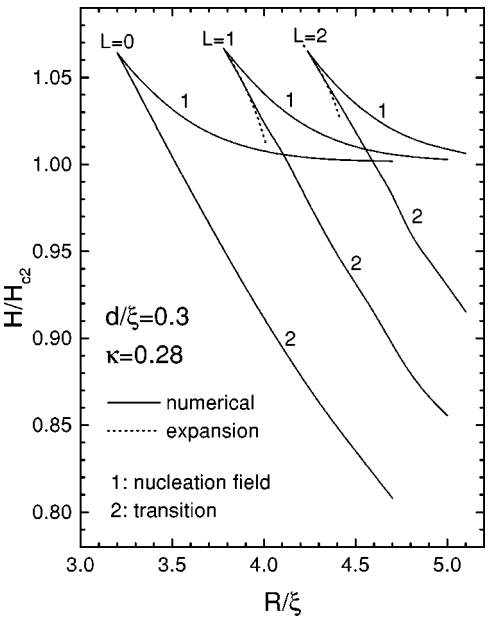


FIG. 22. The nucleation (1) and the critical (2) magnetic fields corresponding to the first-order phase transitions between different superconducting states as functions of the radius of the disk for $d/\xi=0.3$, $\kappa=0.28$ and different angular momenta $L=0,1,2$. Dotted curves show the results of our analytical calculations.

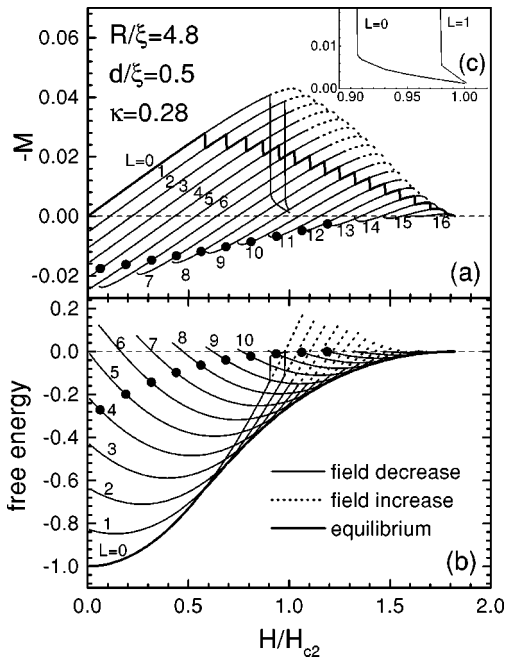


FIG. 23. The magnetization (a) and the Gibbs free energy (b) as function of the magnetic field for a disk with $d/\xi=0.5$, $\kappa=0.28$, $R/\xi=4.8$ (a). Thin solid and dotted curves correspond to increasing and decreasing magnetic fields, respectively. Thick curves correspond to the equilibrium state with minimum free energy. Inset (c) shows the magnetization of the disk for the superconducting states with $L=0,1$ in decreasing magnetic field.

between regions $B>0$ and $B<0$ the system finds itself in the region I, where $A>0$ and a weak superconducting state arises after the transition from the normal state. To understand the reason for the appearance of the first-order transition between the superconducting states, we have to consider how the coefficients $A$ and $B$ depend on the magnetic field. The boundaries of the region I are presented in the inset of Fig. 21(a) for three different values of the magnetic field $H/H_{nuc}=0.95,0.90,0.85$. With decreasing magnetic field the area of region I shrinks. Therefore, the system passes to a region with negative values of the coefficient $A$ resulting in an instability of the weak superconducting state. Unfortunately, to predict quantitatively the value of the critical field corresponding to this transition we must consider higher-order terms in the expansion because the coefficient $A$ changes sign and remains small in absolute value.

The free energy and magnetization of the states with different angular momentum for $d/\xi=0.5$ and $R/\xi=4.8$ are shown in Fig. 23 for increasing and decreasing magnetic field. The considered disk thickness is larger than its critical value and there are prominent jumps in the free energy and magnetization indicating first-order transitions between the superconducting and the normal states. The states with $L=0,1$ exhibit the most interesting behavior in decreasing magnetic field, when the system goes from the normal state to the superconducting state. In accordance with the results of the above analysis, there are weak jumps in the free energy and the magnetization at the nucleation field. Further decreasing the magnetic field leads to a first-order transition to another strong superconducting state. Unfortunately, the peculiarities in the phase transition of a disk with large radius, when the same system exhibits two different adjacent types of transitions, are found for states that are strongly unfavorable. Therefore, the question about the possibility to observe experimentally this interesting metastable behavior still remains to be investigated.

## VII. CONCLUSION

We have presented an analytical approach allowing us to find the critical disk thickness corresponding to switching between second-order and first-order phase transitions of mesoscopic superconducting disks with thicknesses comparable to the coherence and penetration lengths. We considered disks made from a type-I superconductor. When the disk size is relatively small and expulsion of the magnetic field from the disk is not that essential, the system exhibits a behavior inherent for type-II superconductors. In this case, the phase transition between the superconducting state and the normal state are reversible and there are no jumps in the free energy and the magnetization. Thus, we are dealing with second-order phase transitions in thin disks. When the disk thickness exceeds some critical value, the system exhibits features like hysteresis behavior and jumps in the free energy and the magnetization, which are characteristic of first-order phase transitions. We have derived analytical expressions allowing us to find the system characteristics in the vicinity of the critical disk thickness. The obtained results correlate well with our full numerical solution of the GL equations that we performed using finite-difference techniques where the two Ginzburg-Landau equations were solved. We have found that for a large disk radius there are two different steps in the phase transition. The second- or first-order transition between the normal and weak superconducting states can be followed by a new first-order transition between weak and

strong superconducting states with the same angular momentum. The present results are derived for circular disks. If this circular symmetry is broken (see Appendix A) there is a mixing of the different $L$ states and the above transitions between the different $L$ states will be smoothened out.

## ACKNOWLEDGMENTS

This work was supported by the Flemish Science Foundation (FWO-VL) through project 5.0277.97, the project INTAS-93-1495-ext and the ''Interuniversity Poles of Attraction Program - Belgian State, Prime Minister's Office - Federal Office for Scientific, Technical and Cultural Affairs.'' During this work we have benefited from stimulating discussions with A. K. Geim and P. S. Deo.

## APPENDIX A: NUCLEATION FIELD IN ELLIPTICAL AND RECTANGULAR SAMPLES

The experimentally observed sequences of jumps in the magnetization of large radius disks are transitions between different angular momenta that for the axial symmetric case are good quantum numbers. Deviations from the axial symmetry caused by changing the sample shape leads to mixing of states with different angular momentum and, finally, to a removal of the jumps. To treat quantitatively the behavior of a noncircular sample we calculate numerically the lowest eigenfunction and eigenvalues of the linearized first GL equation

$$\hat{L}_{2D}\Psi \equiv (-i\vec{\nabla}-\vec{A}_0)^2\Psi = \lambda\Psi, \tag{A1}$$

for samples with different shapes. Representing the operator $\hat{L}_{2D}$ on a Cartesian space grid, we apply the following iteration procedure $\hat{L}_{2D}\Psi^i=\Psi^{i-1}$ allowing us to find the ground state of $\hat{L}_{2D}$. The last equation was solved numerically. We considered two types of samples: (1) elliptical shaped systems with different aspect ratios $\beta$=1,1.5,2, and (2) rectangles with a different aspect ratio (i.e., the ratio of the sides) $\beta$=1,1.5,2. For $\beta$=1 the first and second cases correspond to samples of circular and square shape, respectively. The area of the samples with different values of $\beta$ was kept the same. The nucleation magnetic fields are shown for different samples in Fig. 24 and are found from the condition $\lambda$=1. Note that jumps in the nucleation field remain in elliptic and rectangle samples with $\beta$=1.5 and are removed only in samples with a larger aspect ratio. As expected, the nucleation field in elliptical samples with the same area increases with a reduction of the radius of curvature. This is similar for the rectangular samples where $H_{nuc}$ increases with $\beta$.

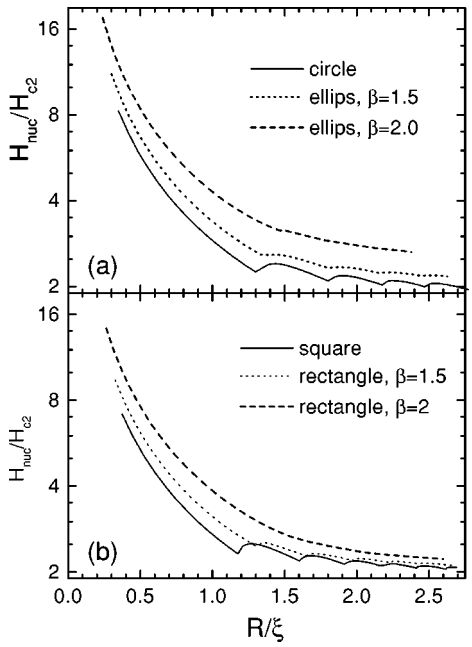


FIG. 24. The upper nucleation field in elliptical (a) and rectangular (b) shaped samples, where $\beta$ denotes the aspect ratio of the axes.

*Permanent address: Institute of Theoretical and Applied Mechanics, Russian Academy of Sciences, Novosibirsk 630090, Russia.
†Electronic address: peeters@uia.ua.ac.be

[1] W. A. Little and R. D. Parks, Phys. Rev. Lett. **9**, 9 (1962); Phys. Rev. **133**, A97 (1964).
[2] A. Bezryadin, A. Buzdin, and B. Pannetier, Phys. Rev. B **51**, 3718 (1995).
[3] O. Buisson, P. Gandit, R. Rammel, Y. Y. Wang, and B. Pannetier, Phys. Lett. A **150**, 36 (1990).
[4] A. K. Geim, S. V. Dubonos, J. G. S. Lok, I. V. Grigorieva, J. C. Maan, L. T. Hansen, and P. E. Lindelof, Appl. Phys. Lett. **71**, 2379 (1997); A. K. Geim, I. V. Grigorieva, S. V. Dubonos, J. G. S. Lok, J. C. Maan, A. E. Filippov, F. M. Peeters, and P. S. Deo, in Proceedings of the 12th International Conference on Electronic Properties of Two Dimensional Systems [Physica B (to be published)].
[5] V. V. Moshchalkov, X. G. Qiu, and V. Bruyndoncx, Phys. Rev. B **55**, 11 793 (1997).
[6] P. G. de Gennes, *Superconductivity of Metals and Alloys* (Addison-Wesley, New York, 1989).
[7] A. K. Geim, I. V. Grigorieva, S. V. Dubonos, J. G. S. Lok, J. C. Maan, A. E. Filippov, and F. M. Peeters, Nature (London) **390**, 259 (1997).
[8] P. S. Deo, V. A. Schweigert, F. M. Peeters, and A. K. Geim, Phys. Rev. Lett. **79**, 4653 (1997).
[9] A. I. Buzdin and J. P. Brison, Phys. Lett. A **196**, 267 (1994).
[10] R. B. Dingle, Proc. R. Soc. London, Ser. A **211**, 500 (1952).
[11] J. D. Jackson, *Classical Electrodynamics* (Wiley, New York, 1962).
[12] A. E. Koshelev and A. I. Larkin, Phys. Rev. B **52**, 13 559 (1995).